Electron-impact excitation of the Mg atom from the ground and metastable states: *R*-matrix calculation with pseudostates

V. Gedeon and V. Lengyel
Department of Theoretical Physics, Uzhgorod State University, Uzhgorod 294000, Ukraine

O. Zatsarinny
Institute of Electron Physics, Uzhgorod 294016, Ukraine

C. A. Kocher
Department of Physics, Oregon State University, Corvallis, Oregon 97331

(Received 1 October 1998)

The recently developed *R*-matrix method with pseudostates (in a 19-state close-coupling approximation) has been applied in the calculation of integral cross sections for electron-impact excitation of neutral Mg. A configuration interaction representation with frozen core is used for the outer electrons. Results are presented for transitions from both the $(3s^2)^1S$ ground state and the $(3s3p)^3P$ metastable state to the 13 lowest-excited target states (with principal quantum numbers $n=3,4,5$), as well as elastic cross sections. Incident electron energies range from threshold to 30 eV. Interpretations are given, with emphasis on comparison of absolute values of the theoretical and measured cross sections and their energy dependence in the near-threshold region. [S1050-2947(99)04603-X]

PACS number(s): 34.80.Dp, 34.80.Pa, 34.50.Fa, 31.25.Jf

I. INTRODUCTION

Accurate values of the cross sections for slow-electron collisions with neutral atomic magnesium, as well as with other alkaline-earth atoms, are of great practical importance in plasma physics (see, e.g., Ref. [1]). When the literature is surveyed for Mg and for Ca, Sr, and Ba, it is immediately apparent that fewer papers (both theoretical and experimental) have been published for Mg. Evidently this neglect of Mg is associated with capricious features of the Mg atom which are not easily modeled, in spite of its seeming simplicity. The calculations presented here are intended to complement and extend the theoretical studies described in the literature, and to encourage further experimental work.

Almost no theoretical explanation has been given for the results of experiments carried out in the 1970s which give integrated excitation cross sections for the low-lying states of Mg [2–4]. The electron-impact excitation function for the $3\ ^1P$ state was determined (by measuring the 285.2 nm resonance radiation) initially by Aleksahin *et al.* [2] and later by Leep and Gallagher [3]. The latter normalized their cross-section measurements to the Born values of Robb [5] using his values for the cascade contribution. Shpenik *et al.* [4] studied the threshold region using a trochoidal electron monochromator with higher electron-beam energy resolution. The measurements of Aleksahin *et al.* [2] are absolute, but their values lie about 40% below those of Leep and Gallagher [3]. Aleksahin *et al.* [2] also obtain cross sections for 37 additional lines of Mg and show excitation functions for 9 of these, including the intercombination line from the $3\ ^3P_1$ level. The values quoted are much smaller than the Born approximation would suggest. Shpenik *et al.* [4] also show excitation functions for eight other lines. With their higher-energy resolution (half-width 0.1 eV), they observed several sharp structures in the excitation functions at impact energies below 10 eV, which they attribute to the decay of short-lived autodetaching states of the negative Mg^- ion.

Low-energy elastic scattering of electrons by Mg was studied by Burrow and Comer [6] by means of electron transmission experiments. They reported a strong shape resonance at 0.15 eV. These results have been supported by high-resolution measurements (with half-widths 0.03–0.05 eV) by Romanyuk *et al.* [7], who also determined absolute values for the total cross section in the range from 0.1 to 10 eV and observed an additional resonance at the threshold of the $3\ ^3P$ level.

In addition, there have been recent experimental efforts in measuring excitation cross sections from the metastable levels of alkaline-earth atoms [8,9]. Absolute values for the excitation cross sections have been obtained for five transitions from the $3\ ^3P_{0,2}$ metastable state of Mg [10]. We should also note the measurement of differential cross sections for Mg, as well as coherence and correlation parameters [11]. These recent experimental efforts [12] have served to stimulate interest in the corresponding theoretical work [13].

In view of the long lifetimes of the metastable states (in some cases above 10^{-5} s) and also the large expected values of the corresponding cross sections (typically $10^{-15}\,\mathrm{cm}^2$), one expects these processes to play a fundamental role in a variety of plasma and laser devices.

Electron-impact excitation of Mg is also of considerable interest from the theoretical standpoint. A primary reason is that Mg is a relatively simple atom, in which both the ground state and the excited states can be well described within the *LS* coupling formalism. On the other hand, Mg as a target in electron-impact processes shows significantly different behavior when compared to He, a much-studied target in electronic collisions. While the ground state of Mg is also a closed-shell ^1S state, it shows strong electron correlation effects, and the low-lying optically allowed transitions are

strongly coupled to each other. Therefore it is interesting to investigate the influence of these features on the various observables that can be extracted from electron scattering experiments.

As noted above, very little theoretical attention has been devoted to studies of the integrated cross sections for Mg. Apart from the pioneering work of Fabrikant [14], which uses a simple three-state close-coupling approximation, only the works of Mitroy and McCarthy [15] and McCarthy *et al.* [16] deal with this topic. These works employed a coupled-channel optical method in five- and six-state approximations to study the differential and integrated cross sections for elastic and inelastic ($3\ ^1P$ and $3\ ^3P$) scattering at 10, 20, and 40 eV. Clark *et al.* [17] used first-order many-body theory (FOMBT) and a distorted-wave approximation (DWA) to study the influence of configuration mixing of the target-state wave functions in the case of excitation from the $n \leqslant 3$ states. None of these theoretical calculations, however, are consistent with the experiments over a wide range of scattering angles and energies. In this connection it is clear that new, accurate calculations of total cross sections, and the detailed analysis of excitation functions, are a significant undertaking with fundamental scientific interest as well as value for practical applications. Comparison of the cross sections for Mg with the similar results for Ca and Sr is a further interesting prospect, providing insight into the whole alkaline-earth-group.

It is surprising that no calculations have been undertaken within the framework of such a widely used method as the *R*-matrix approximation. One possible reason may be that the appearance of excessive pseudoresonance structure plagues the results of *R*-matrix calculations for complex atoms [18]. This problem arises from difficulties in maintaining consistency when the *N*-electron target is incorporated into the $(N+1)$-electron collision problem. In addition, it is recognized that achieving accurate cross sections at intermediate energies requires the inclusion of the target continuum in the close-coupling expansion. These problems have been attacked in recent calculations by Bartschat *et al.* [19,20], using the *R* matrix with pseudostates (RMPS) method. The RMPS method is an extension of the *R*-matrix method [21] which uses a pseudostate representation of the target continuum in order to incorporate the ionization channels into the *R*-matrix calculations. The great advantage of the *R*-matrix approach, inherited from the basic *R*-matrix method, is the ability to generate accurate results on a fine energy mesh after the single time-consuming step of solving the problem within the ''inner'' region. Thus far, its primary limitations are that the physical states need to fit within the *R*-matrix radius, making the application to extended target states difficult, and that the functional expansion used in describing the projectile electron makes the method inappropriate beyond some energy, in the intermediate- to high-energy range. However, most importantly, the RMPS method takes the target continuum into account and thus is able to yield accurate results over a much larger energy range than the standard *R*-matrix method.

Besides the RMPS approach, the convergent close-coupling (CCC) method, first developed for hydrogen [22] and later applied with great success to elastic and inelastic electron collisions with other quasi-one-electron systems [23] as well as helium [24], seems to be a very promising method for attacking this problem. The CCC computer code has recently been extended to handle two electrons outside a closed core [25]. This method is characterized by simultaneous consideration of both excitation and ionization, and by the additional inclusion of the continuum in the set of target states. The coupled target states are defined by diagonalizing the Hamiltonian in a square-integrable orthogonal Laguerre basis, where the negative-energy states provide the representation of the true discrete spectrum and the positive-energy states discretize the continuum. The CCC method concentrates on a single energy at a time, but it is able to treat high-lying excited states and it is applicable at all energies. For this reason, examining the scattering problem jointly—with RMPS at low and intermediate energies and CCC at intermediate and high energies—provides a very good way to obtain accurate results for the cross sections. This approach has recently been demonstrated in the case of $e+$Be scattering [25]. In the case of $e+$Mg, only differential cross sections have been calculated so far [26].

In this paper we present the results of 19-state RMPS calculations (19CC) for $e+$Mg scattering. The target states are represented by configuration-interaction (CI) wave functions and include the 13 low-lying bound states of Mg with principal quantum numbers $n \leqslant 4$, as well as the $(4s5s)^{1,3}S$ states. The present work is a continuation and development of a series of works devoted to calculations of electron scattering by alkaline-earth atoms and ions in the near-threshold-energy region, from both the ground state and the metastable states [9,27–29]. These investigations are directed toward the analysis and interpretation of measurements of integral cross sections undertaken at Uzhgorod State University which have had no theoretical interpretation until now. The corresponding differential cross sections, as well as detailed analyses of the resonance structure, will be analyzed and presented in future publications.

II. DETAILS OF CALCULATIONS

The total wave function used in the *R*-matrix method [21] to describe the collision in the inner region, $r<a$, where exchange between the projectile and the target electrons is not negligible, can be written as an expansion in terms of a set of basis functions.

$$\Psi_k(\mathbf{r}_1,\ldots,\mathbf{r}_N,\mathbf{r}) = A\sum_{ij} a_{ijk}\Phi_i(\mathbf{r}_1,\ldots,\mathbf{r}_N,\hat{\mathbf{r}},\sigma)\frac{1}{r}u_j(r) + \sum_j b_{jk}\phi_j(\mathbf{r}_1,\ldots,\mathbf{r}_N,\mathbf{r}). \quad (1)$$

Here the Φ_i are channel functions formed from all the target states (physical and pseudo) included in the expansion, the $u_j(r)$ are continuum orbitals that describe the motion of the scattering electron, and the ϕ_i are $(N+1)$-electron bound configurations, constructed from the target configurations plus another target orbital. The second sum in Eq. (1) includes at least those configurations that are required to compensate for orthogonality constraints imposed on the radial solutions $u_j(r)$. Finally, $\hat{\mathbf{r}}$ and σ denote the angular and spin coordinates of the projectile, and the operator *A* ensures full

antisymmetrization of the wave functions. The coefficients a_{ijk} and b_{jk} were found by diagonalizing the $(N+1)$-electron Hamiltonian inside the R-matrix box, of radius a. To perform the present scattering calculations, we used the RMATRIX1 program [30].

The channel functions Φ_i are the input parameters for this program. It is well known that the Hartree-Fock model does not provide a good description of the ground and excited states of neutral alkaline-earth atoms. Since an adequate description of the atomic structure is a prerequisite for an accurate scattering calculations, we have chosen to represent the Mg ground and excited states by CI wave functions. On other hand, as mentioned previously, an important consideration with regard to the occurrence of pseudoresonances in R-matrix calculations is the need for a consistent description of the N-electron target within this $(N+1)$-electron collision problem. There is no unique recipe for achieving this goal, but a good approximation is obtained if one additional electron is coupled to every important configuration in the target description and if the close-coupling expansion (1) contains the maximum number of target physical states and pseudostates [20,31]. In extended calculations like the present one, it can become difficult to limit the matrix dimension to a tractable size. Accordingly, it is necessary to apply some restrictions to the basis states used in CI description of the target states.

A. Target states

A good systematic representation of wave functions for atoms with two valence electrons may be achieved in a frozen-core approximation by using the corresponding ionic orbitals for construction of the basis functions and introducing a phenomenological polarization potential for the core, to take into account the core-valence correlation. This variant of the CI method reduces the problem to a two-electron calculation and has been widely used in a variety of calculations. We have used this method for representing the target wave functions for $e+\mathrm{Ca}$ [9] and $e+\mathrm{Sr}$ [27] scattering, as well as for representing the autoionizing states in the cases of $e+\mathrm{Ca}^+$ scattering [28] and two-photon ionization of Mg [32]. The details of these calculations are given in the above references. The scheme of calculation can be outlined as follows.

The Hamiltonian of the quasi-two-electron target can be written as

$$H_T = H_1 + H_2 + V_{12}, \tag{2}$$

where H_i is the one-electron Hamiltonian for the ith electron above the Hartree-Fock core, corrected by a phenomenological polarizationlike potential V^{pol}, so that

$$H_i = K_i + V_i = -\tfrac{1}{2}\nabla_i^2 + V_i^{\mathrm{FC}} + V_i^{\mathrm{pol}}, \tag{3}$$

and the two-electron potential V_{12} is taken to be a sum of the electron-electron potential and the di-electron polarization potential $V^{\mathrm{di\text{-}el}}$:

$$V_{12}(\hat{r}_1\cdot\hat{r}_2) = 1/|r_i - r_j| + V_{12}^{\mathrm{di\text{-}el}}(\hat{r}_1\cdot\hat{r}_2). \tag{4}$$

The latter interaction simulates the effects of mutual polarization of the core by the two valence electrons. If V_{12} is considered as a perturbation, then the calculations consist of the following steps. First, the nonlocal frozen-core Hartree-Fock potential V^{FC} is generated by performing a self-consistent-field Hartree-Fock calculation for the Mg^{++} ion, for which we define the orbitals $1s$, $2s$, and $2p$. Then the set of one-particle orbitals, nl, is generated from the frozen-core Hartree-Fock calculations for the $2p^6nl$ states of Mg^+. In performing this step, we can also obtain the parameter for the polarization potential V^{pol} from the condition that the binding energies for some low-lying states $2p^6nl$ coincide with experimental data. Then the complete wave function of the atom is expanded over a basis of states in which only the outer orbitals are changed:

$$\Psi^{LS} = \sum_{i=(nl,n'l')} c_i \Phi_i^{LS}(1s^2 2s^2 2p^6\mathrm{core}, nl, n'l'). \tag{5}$$

The energies of the atomic states and the corresponding expansion coefficients c_i are then obtained by the diagonalization of V_{12}. The size of the basis is chosen for accurate replication of the energies for some selected states in each atomic Rydberg series under consideration. In the present calculations, the set of basis functions in Eq. (5) for a given LS term includes 80 to 120 states with the $3snl$, $3pnl$, $3dnl$, $4snl$, $4pnl$, and $4dnl$ configurations ($n\leqslant 15, l\leqslant 4$), plus some other higher-lying configurations $nln'l'$ with comparable values of the quantum numbers n and n'. V^{pol} and its parameters used in the present calculations are given in [32].

An energy level diagram for Mg, showing a number of the relevant levels, is presented in Fig. 1. Table I lists the

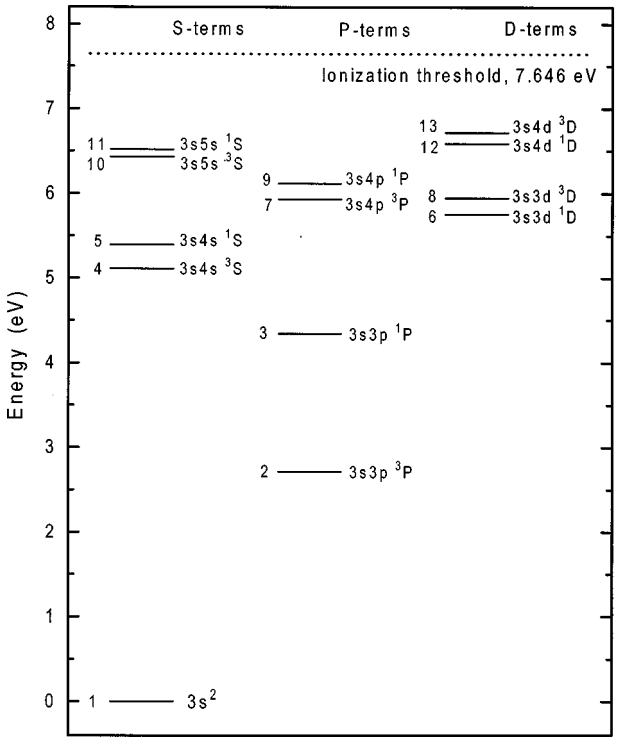

FIG. 1. Simplified energy level diagram for Mg, showing levels involved in the present scattering calculations.

TABLE I. Binding energies (in Ry) of the physical target states of neutral Mg, relative to the Mg^+ series limit.

State	Experiment [33]	MCHF [34]	Present calculations: Full basis	Present calculations: Reduced basis
$(3s^2)^1S$	−0.5620	−0.5532	−0.5557	−0.5426
$(3s3p)^3P^0$	−0.3625		−0.3589	−0.3541
$(3s3p)^1P^0$	−0.2426	−0.2390	−0.2389	−0.2317
$(3s4s)^3S$	−0.1865		−0.1862	−0.1809
$(3s4s)^1S$	−0.1655	−0.1643	−0.1629	−0.1571
$(3s3d)^1D$	−0.1391	−0.1422	−0.1378	−0.1359
$(3s4p)^3P^0$	−0.1260		−0.1249	−0.1205
$(3s3d)^3D$	−0.1250		−0.1242	−0.1204
$(3s4p)^1P^0$	−0.1123	−0.1113	−0.1108	−0.1066
$(3s5s)^3S$	−0.0893		−0.0890	−0.0845
$(3s5s)^1S$	−0.0831		−0.0819	−0.0769
$(3s4d)^3D$	−0.0778		−0.0771	−0.0736
$(3s4d)^1D$	−0.0681		−0.0678	−0.0639

binding energies for the Mg states involved in the present scattering calculations, together with those calculated in the multiconfigurational Hartree-Fock scheme (MCHF, Ref. [34]) and with results from the available experimental data [33]. The largest discrepancy between the computed and experimental energies is 0.006 Ry for the ground state, decreasing for higher-lying levels. For the majority of the levels, the difference between theory and experiment is less than 0.001 Ry. The accuracy obtained is comparable with that for the large-basis MCHF values of Froese Fischer [34]. Note also that the introduction of the polarization potential considerably improves the accuracy of the binding energies.

Another, much more sensitive test of the quality of the target wave functions can be obtained by comparison of the optical oscillator strengths for allowed dipole transitions. Table II compares the present result (full basis) for absorption oscillator strengths with experimental values and with the MCHF values [34]. The present values were obtained using the theoretical energies and a modified form of the dipole operator which includes core-polarization corrections (see, for example, [28]), but the polarization corrections here, in contrast to the cases of Ca and Sr [9,27], are rather small and do not exceed 3%. On the whole, very good agreement is obtained between the present calculated values of the oscillator strengths and the MCHF values. Both sets of results are also in close agreement with the experimental values [35]. Note that only minor differences remain between the length and the velocity values of the oscillator strengths.

We may conclude that the success of the above variant of the CI method results from the use of accurate target wave functions, but they cannot be directly incorporated into the *R*-matrix calculations for a number of reasons. First, the convergence of the multiconfigurational expansion (5) is rather slow, and for accurate results it needs to include basis functions $\Phi(nln'l')$ with large values of the principal quantum number n'. As a consequence, we would require an excessively large *R*-matrix box radius *a*. Second, the large size of the expansions (5) and the large number of incorporated one-particle orbitals *nl* leads to large expansions over the bound states in Eq. (1) and makes the electron scattering calculations prohibitively time consuming. Third, and most important, it also leads to a very prominent pseudoresonance structure which may completely distort the functional form of the cross sections at intermediate scattering energies.

For this reason we restricted the target expansions (5) in the following *R*-matrix calculations by including only the terms with expansion coefficients $c_i > 0.05$. This simplification considerably reduces the number of basis functions, leaving the following 17 configurations in the description of the lowest 13 target states involved in the scattering calculations: $3s^2$, $3s4s$, $3s5s$, $3s6s$, $3s3d$, $3s4d$, $3s5d$, $3s6d$, $3p^2$, $3p4p$, and $3p4f$ (even states), plus $3s3p$, $3s4p$, $3s5p$, $3p4s$, $3p3d$, and $3p4d$ (odd states). The resulting binding energies and oscillator strengths are included in Tables I and II under the heading ''Reduced basis.'' We note that the new binding energies are affected by an additional shift of up to 0.01 Ry which we believe does not significantly affect the scattering results. Much more significant shifts are observed for the oscillator strengths, most notably for transitions involving the higher-lying $3s5s$, $3s4p$, and $3s4d$ states. However, for transitions from the $(3s^2)^1S$ ground state and the $(3s3p)^3P$ metastable states, which are under study in the present work, the reduced-basis oscillator strengths differ only moderately from the full-basis results, providing strong evidence that the accuracy of the reduced basis is sufficient for the representation of the target states in the present scattering calculations.

B. Collision calculations

As demonstrated in the RMPS works on $e+\mathrm{Be}$ scattering [20], it is advantageous to keep as many target states as possible in the close-coupling expansion (1), in order to control the effect of pseudoresonances. In total, the above-mentioned configurations in the reduced basis give rise to 40 target states, taking into account the $LS\pi$ structure. It is convenient to divide these states into 13 physical states with energies corresponding to the experimental ones and 27 pseudostates with energies lying close to the ionization threshold and in the adjacent continuum. The latter are included in the close-coupling expansion in order to (i) represent the coupling to the target continuum and (ii) control the effect of unphysical resonances. Although pseudoresonances can still occur due to the thresholds associated with the pseudostates, their effect can be drastically reduced by keeping as many states as possible in the expansion [31]. But our control calculations show that the pseudoresonance structure is considerably reduced already with the inclusion of only one pseudostate for each target symmetry, and the further addition of other pseudostates only slightly affects the resulting cross sections. Therefore, to save computation time in our final calculations, we retained in the close-coupling expansion (1) all 13 physical states and one pseudostate for each angular symmetry of the target. All these pseudostates have energies close to the ionization threshold and are assumed to simulate the rest of the physical states of Mg not included in the close-coupling expansion. In all, we have 19 states in the first sum of expansion (1): 13 physical states and 6 pseudostates. The latter lie close to the ionization threshold.

The remaining small oscillations in the cross sections above the ionization threshold were eliminated by convolut-

TABLE II. Oscillator strengths for transitions between states of the Mg target. Values for the length and velocity gauges are denoted by f_l and f_v, respectively. Experimental errors in the final digits are shown in parentheses.

Transition	Present calculations: Full basis f_l	Full basis f_v	Reduced basis f_l	Reduced basis f_v	MCHF [34] f_l	MCHF [34] f_v	Experiment	Branching ratio
$(3s^2)^1S$-$(3s3p)^1P^0$	1.771	1.698	1.734	1.693	1.757	1.736	1.83(8)[a], 1.83(18)[b] 1.75(7)[c], 1.80(5)[d] 1.86(3)[e], 1.66(16)[f]	1.0
$(3s^2)^1S$-$(3s4p)^1P^0$	0.124	0.109	0.136	0.119	0.117	0.114	0.19(2)[a], 0.1022(2)[d] 0.18(4)[e], 0.109(8)[g]	0.854
$(3s3p)^3P^0$-$(3s4s)^3S$	0.139	0.134	0.139	0.145				1.0
$(3s3p)^3P^0$-$(3s5s)^3S$	0.016	0.015	0.041	0.012				0.755
$(3s3p)^3P^0$-$(3s3d)^3D$	0.627	0.617	0.613	0.580				1.0
$(3s3p)^3P^0$-$(3s4d)^3D$	0.126	0.123	0.204	0.115				0.839
$(3s3p)^1P^0$-$(3s4s)^1S$	0.158	0.146	0.166	0.116	0.155	0.155		1.0
$(3s3p)^1P^0$-$(3s5s)^1S$	0.007	0.006	0.027	0.005				0.405
$(3s3p)^1P^0$-$(3s3d)^1D$	0.256	0.254	0.248	0.260	0.206	0.212	0.34(2)[g]	1.0
$(3s3p)^1P^0$-$(3s4d)^1D$	0.102	0.101	0.060	0.090				0.710
$(3s4s)^3S$-$(3s4p)^3P^0$	1.340	1.301	1.390	1.441				1.0
$(3s4s)^1S$-$(3s4p)^1P^0$	1.271	1.214	1.330	1.234	1.236	1.240		0.128
$(3s3d)^1D$-$(3s4p)^1P^0$	0.139	0.131	0.150	0.151	0.137	0.140		0.019
$(3s4p)^3P^0$-$(3s3d)^3D$	0.020	0.023	0.006	0.041				0.000
$(3s4p)^3P^0$-$(3s5s)^3S$	0.286	0.277	0.313	0.271				0.242
$(3s4p)^3P^0$-$(3s4d)^3D$	0.627	0.613	0.613	0.653				0.161
$(3s4p)^1P^0$-$(3s5s)^1S$	0.233	0.229	0.259	0.335				0.595
$(3s4p)^1P^0$-$(3s4d)^1D$	0.940	0.930	0.820	1.210				0.290

[a]Reference [35(a)].
[b]Reference [35(b)].
[c]Reference [35(c)].
[d]Reference [35(d)].
[e]Reference [35(e)].
[f]Reference [35(f)].
[g]Reference [35(g)].

ing the results with a Gaussian with energy resolution $\Delta E = \sqrt{e}$, where e is the energy (in Rydbergs) above the ionization threshold. Such a procedure was suggested and applied successfully by Meyer *et al.* [36] to smooth out the remaining pseudostructures in numerically calculated results.

As discussed above, the sum over bound channels in Eq. (1) must include all $(N+1)$-electron states that have parent terms included in the first summation—not more, not less—and this point is crucial for obtaining correct energies for the $(N+1)$-electron system and accurate energy dependences for the cross sections in near-threshold region, especially for weak exchange transitions. Following this prescription is also very important for reducing the pseudostructure discussed above. In our calculations, an automatic procedure was developed for carrying out the cumbersome selection process for the bound channels.

R-matrix calculations were carried out with the following parameters: *R*-matrix radius $a = 60a_0$, a total of $N^{\text{cont}} = 20$ continuum basis functions $u_j(r)$ for each orbital angular momentum, and a range $0 \leqslant l \leqslant 14$ for the orbital angular momenta of the scattered electron. The *R*-matrix calculation with full inclusion of exchange was carried out for all partial waves with $L \leqslant 12$, and partial wave contributions for $L > 12$, if necessary, were estimated by a top-up procedure via a geometric series.

For completeness, we also carried out the calculations in a plane-wave Born-Ochkur approximation (PWBOA) for all transitions under study, in order to examine the influence of the distortion potential and the coupling between scattering channels on the excitation cross sections. The relevant formulas are given in [9].

III. RESULTS AND DISCUSSION

A. The $(3s^2)^1S$-$(3s3p)^1P$ transition

The resonance transition $(3s^2)^1S$-$(3s3p)^1P$ has been studied extensively and is well described in the literature. Table III and Figs. 2(a) and 2(b) compare our results with other selected theoretical results and with the experimental data available. The PWBOA cross sections are considerably greater than those from the close-coupling calculations and are comparable with the DWA cross sections. Unitarization

TABLE III. Comparison of theoretical and experimental results for the integral cross sections (units of 10^{-16} cm^2) for electron-impact excitation of the 3 ^1P and 3 ^3P states of Mg.

	$3s^2\ ^1S-3s3p\ ^1P$		$3s^2\ ^1S-3s3p\ ^3P$	
	10 eV	20 eV	10 eV	20 eV
Theory				
PWBOA[a]	27.4	25.9	5.18	0.65
DWA[b]	28.8	25.6	5.37	0.67
UDWA[c]	19.7	20.6	4.69	0.66
5CC[d]	17.6	18.7		
6CC[e]	16.7	18.9	3.63	0.67
6CCO[f]	17.0	15.5	3.79	0.61
19CC[g]	12.8	14.5	1.94	0.44
Experiment				
Aleksahin *et al.* [2]	6.77	8.52	2.59	0.83
Leep and Gallagher [3]	14.1	15.2		
Williams and Trajmar [11]	14.0	15.0	3.10	0.80
Shpenik *et al.* [4]	12.9			
Houghton *et al.* [12]			2.83	0.51

[a]Present plane-wave Born-Ochkur approximation results (with full basis for target states).
[b]Distorted-wave approximation results of Clark *et al.* (Ref. [17]).
[c]Unitarized DWA results of Clark *et al.* (Ref. [17]).
[d]Five-state coupled-channel calculation by Mitroy and McCarthy (Ref. [15]).
[e]Six-state coupled-channel calculation by McCarthy *et al.* (Ref. [16]).
[f]Six-state optical-potential calculation by McCarthy *et al.* (Ref. [16]).
[g]Present 19-state RMPS results.

(UDWA) has a strong effect on the integral cross sections at low energies and decreases the results below the nonunitarized values by about 30% at an incident electron energy of 10 eV. It indicates that the weak-coupling conditions required for the applicability of PWBOA and DWA are not satisfied in the case of Mg. In spite of this situation, the Mg atom is well described by *LS* coupling. The channel coupling at low energies is important not only among the singlet or triplet subsystems but also between singlet and triplet states. This effect is evident in a comparison of the 5CC and 6CC results, which differ by the inclusion of the triplet 3 ^3P level in 6CC which does not appear in the fully singlet expansion 5CC. Our 19CC result is in good agreement with the 6CCO values.

As is seen in Fig. 2(a), there is very satisfactory overall agreement between the present 19CC results and the experimental data by Leep and Gallagher [3]. Since the results from the experiment [3] are reported as emission cross sections, it is necessary to account for population by cascade from the $(3s4s)^1S$, $(3s3d)^1D$, and $(3s4p)^1P^0$ levels. Since the $(3s4p)^1P^0$ level can also decay directly to the ground state, the effective emission cross section is given by

$$\sigma_{\rm em}=\sigma_{3p}+\sigma_{3d}+\sigma_{4s}+0.157\sigma_{4p}\,.$$

The f values from the present calculations were used in evaluating the branching ratios given in Table II. For consistency, the same cascade contribution was added to the PW BOA and DWA cross sections. Note the relatively large cascade contribution for Mg in comparison with the same transition in Ca or Sr [9,27].

The absolute values obtained by Aleksahin *et al.* [2] are systematically lower by about 40–60 % than both the present calculations and the experimental results [3]. The latter data were normalized to the Born calculations by Robb [5] at 1500 eV, while the measurements [2] are absolute. In general, the absolute measurement of cross sections is a challenging task, and the data obtained are scaled to within a factor of 2 [8,9]. The uncertainty in the absolute values for all the cross sections given in [2] was estimated to be 35%, but the above comparison (and the comparison for other transitions discussed below) suggests that the errors in the determination of the absolute values [2] may be much larger, perhaps reaching a factor of 2 or 3.

Our $(3s^2)^1S$-$(3s3p)^1P$ cross section is systematically lower by about 10% than the experimental data [3] at incident electron energies in the range 8–10 eV, but is in very good agreement with the data by Shpenik *et al.* [4]. The latter are only relative measurements and were normalized at an energy of 5 eV to our calculations and to measurements [3] which coincide at this energy. More detailed comparison with experiment [4] is given in Fig. 2(b) on an expanded scale. We see very good agreement in the functional form of the energy dependence in the near-threshold region. As mentioned above, the measurements [4] were made with high energy resolution and are the most accurate relative measurements at the present time. It should also be emphasized that the shape of the cross section for the $(3s^2)^1S$-$(3s3p)^1P$ transition in the near-threshold region is very sensitive to the number of channels included in the close-coupling expansion (1) due to strong coupling to the upper levels. Our control 3CC, 5CC, and 7CC calculations have shown very different energy dependences for the cross sections in the near-threshold region, and the close agreement of our final 19CC calculation with the measurements [4] indicates that convergence of the close-coupling expansion has been achieved in this energy range. Our calculations also reveal some resonance structure in the cross sections. A detailed analysis of this structure, as well as a determination of whether this structure is due to physical or pseudoresonances, is beyond the scope of the present discussion and will be published elsewhere.

B. The $(3s^2)^1S$-$(3s3p)^3P$ transition

A comparison of the available theoretical and experimental results for the intercombination transition $(3s^2)^1S$-$(3s3p)^3P$ is given in Table III and Fig. 3(a). The PWBOA and DWA results are considerably higher than the 6CC and 19CC results at 10 eV, but at 20 eV the values obtained in the first-order approximations are in satisfactory agreement with close-coupling calculations. We can conclude that channel coupling effects in this case are important only for low incident energies, approximately of order of the first ionization threshold. On the other hand, the close agreement between the PWBOA and DWA values indicates that the Born-Ochkur approximation accounts well for the two-

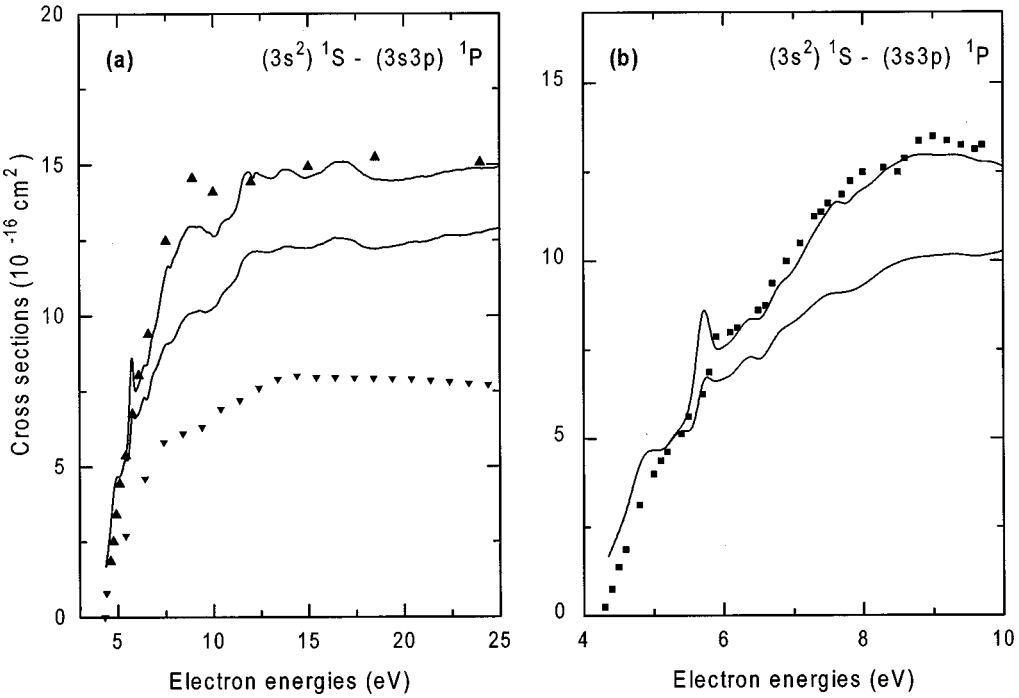

FIG. 2. Comparison of experimental excitation functions with present calculated cross sections for the resonant $(3s^2)^1S$-$(3s3p)^1P$ transition in Mg. ——, 19CC results (upper curve with cascade, lower curve without cascade); ▲, experiment [3]; ▼, experiment [2]; ■, experiment [4].

electron exchange interaction. However, the channel coupling has a much stronger effect here, and as a result, the PWBOA cross section exceeds the 19CC results by factor of 2 at the near-threshold maximum.

As is seen in Table III, the present 19CC results are systematically lower by about 25% than the 6CC results and the experimental data—except near 20 eV, where our value is in close agreement with the data of Houghton *et al.* [12]. The limitations of the experimental accuracy prevent us from reaching a final conclusion about this difference in theoretical results. Figure 3(a) also compares the present results with the absolute measurements by Aleksahin *et al.* [2]. The the-

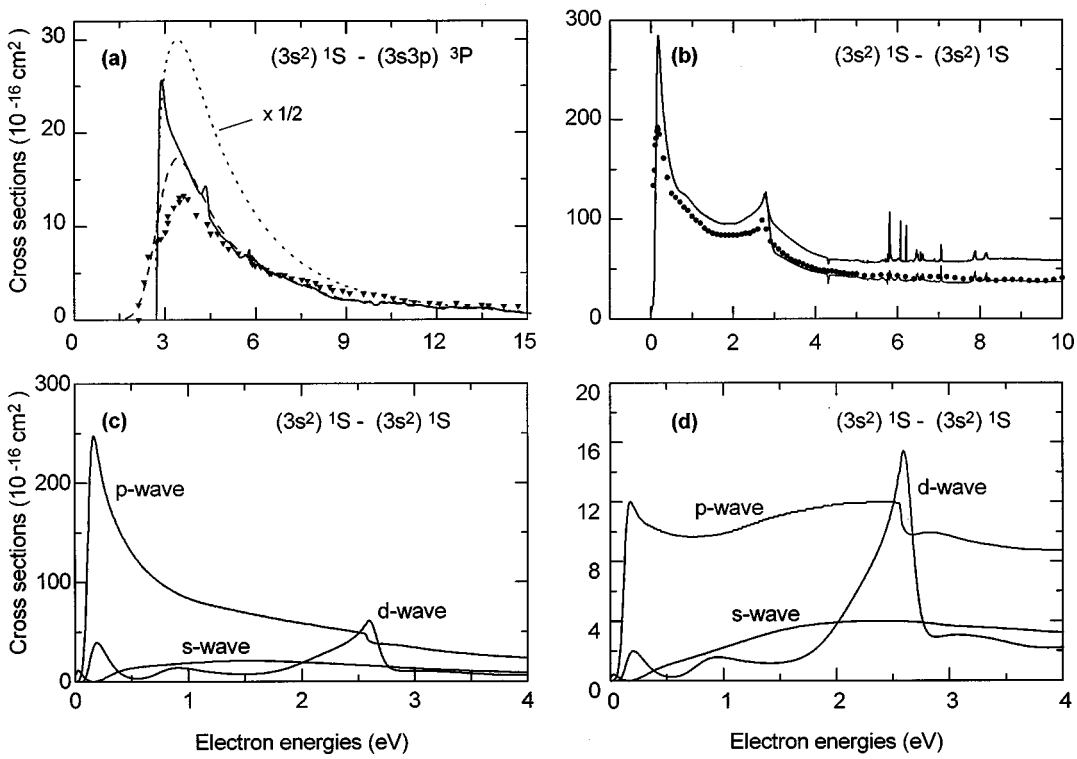

FIG. 3. Comparison of experimental excitation functions with present calculations for the intercombination $(3s^2)^1S$-$(3s3p)^3P$ transition (a) and elastic scattering (b)–(d) in Mg. ——, 19CC results; ------, PWBOA results; ▼, experiment [2]; ●, experiment [7].

oretical cross section reveals a sharp near-threshold maximum, whereas the experiment gives a smooth curve, which may be due to the large energy inhomogeneity (~1.0 eV) of the electron beam in this experiment [2]. If we convolute our calculated result with the experimental electron distribution function, the resulting curve [Fig. 3(a), dashed line] has a shape close to the experimental one, but at its maximum it exceeds the experimental results by about 20%.

C. Elastic and total cross sections for the Mg ground state

Figure 3(b) shows the results from the present calculations for the elastic (lower curve) and total (upper curve) cross sections. Also shown are the absolute measurements of total cross sections by Romanyuk *et al.* [7]. The total cross section has been obtained as a sum of the elastic cross section and all calculated excitation cross sections for the first 13 target levels. We see that there is excellent agreement in the energy dependence of the total cross section, including the two resonancelike maxima at low energies and at the threshold of the $3\ ^3P$ level (2.71 eV). Our absolute values for the total cross section are systematically larger than the experimental data by about 30%, which is within the limit of experimental error [7]. At an electron energy of 10 eV, the absolute value obtained for the elastic cross section, $37\times10^{-16}\,\mathrm{cm}^2$, also agrees fairly well with the experimental value $29\times10^{-16}\,\mathrm{cm}^2$ obtained by Williams and Trajmar [11]. Note for comparison that the 6CCO calculations [15] predict a value $22\times10^{-16}\,\mathrm{cm}^2$.

To elucidate the nature of the maxima in the total cross section, Fig. 3(c) shows the partial-wave contributions to the elastic cross section at low energies. We see that the *P*-wave contribution dominates at low energies and is responsible for the first threshold resonance at 0.17 eV. Its position agrees well with the experimental results, 0.15 eV [16] and 0.16 eV [7]. It is a classical shape resonance and is due to formation of a negative Mg^- ion in the quasibound state $(3s^2 3p)^2P$, which decays to the ground state due to the passage of the $3p$ electron through its potential barrier. It should be noted that in the calculation of elastic cross sections we used the experimental values for the target binding energies because the calculated cross section at such low energies is very sensitive to the position of the resonance due to the singular factor $1/k^2$.

TABLE IV. Comparison of theoretical and experimental results for the integral cross sections (units of $10^{-16}\,\mathrm{cm}^2$) for electron impact excitation of the $3\ ^1D$ and $4\ ^1S$ states of Mg.

	$3s^2\ ^1S-3s3d\ ^1D$		$3s^2\ ^1S-3s4s\ ^1S$	
	10 eV	20 eV	10 eV	20 eV
PWBOA	2.95	2.49	0.930	0.755
DWA	1.51	1.62	4.50	2.39
UDWA	1.49	1.60	3.23	1.85
5CC	1.69	1.49	1.02	0.726
19CC	2.08	1.92	0.380	0.192
Experiment of Williams and Trajmar [11]	0.7	2.1		0.6

The cross section is expressed in terms of the collision strength Ω as

$$\sigma_{if}(E)=\frac{\pi a_0^2}{k_i^2(2L_i+1)(2S_i+1)}\Omega_{if}(E).$$

Figure 3(d) presents the corresponding collision strengths for elastic scattering. Collision strengths are not so sensitive to the details of the calculations and may be useful for further comparison with other calculations. Furthermore, since the collision strengths do not contain the kinematic factor $1/k^2$, they give clearer information about the resonance structure. For example, we see that the second maximum is determined by two factors: the cusp peculiarity in the *P* wave, exactly at the $3\ ^3P$ threshold (2.714 eV), and the shape resonance in the *D* wave, at energy 2.730 eV, slightly above the $3\ ^3P$ threshold. It results similarly from the formation of the $(3s^2 3d)^2D$ quasibound state of the negative Mg^- ion. For detailed discussion of previous results, see [29] and the literature cited therein.

D. The $(3s^2)^1S$-$(3s3d)^1D$ and $(3s^2)^1S$-$(3s4s)^1S$ transitions

Two additional transitions are available for the comparison of results: the quadrupole transition $(3s^2)^1S$-$(3s3d)^3D$ and the monopole transition $(3s^2)^1S$-$(3s4s)^1S$. The relevant data are presented in Table IV and Figs. 4(a) and 4(b).

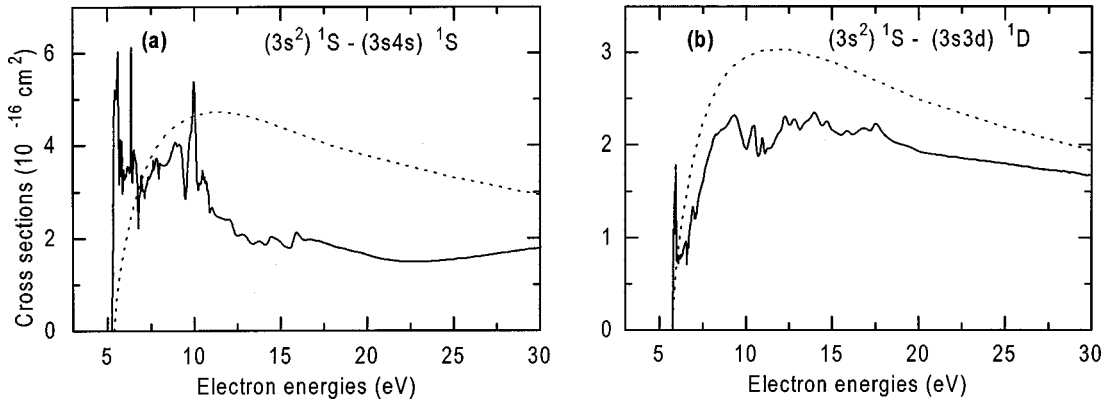

FIG. 4. Excitation cross sections for the monopole $(3s^2)^1S$-$(3s4s)^1S$ (a) and quadrupole $(3s^2)^1S$-$(3s3d)^1D$ (b) transitions in Mg. ——, 19CC results; ------, PWBOA results.

TABLE V. Comparison of theoretical and experimental cross sections (units of $10^{-16}\,cm^2$) for electron-impact excitation of selected states of Mg.

Transition	Energy (eV)	Present calc.	Experiment	
			Aleksahin *et al.* [2]	Snegurskaya [10]
$(3s^2)^1S$-$(3s4s)^3S$	10	0.505	0.935	0.460
	20	0.053	0.103	0.070
$(3s3p)^3P$-$(3s4s)^3S$	10	3.84		8.27
	20	3.87		9.39
$(3s^2)^1S$-$(3s3d)^3D$	10	0.605	0.165	0.330
	20	0.105	0.050	0.066
$(3s3p)^3P$-$(3s4s)^3D$	10	5.07		4.93
	20	6.32		5.88
$(3s^2)^1S$-$(3s5s)^1S$	10	0.107	0.086	
	20	0.099	0.079	
$(3s3p)^3P$-$(3s5s)^3S$	10	0.220		0.245
	20	0.180		0.256
$(3s^2)^1S$-$(3s4d)^1D$	10	0.895	0.150	
	20	0.424	0.107	
$(3s3p)^3P$-$(3s4d)^3D$	10	1.45		0.753
	20	1.60		0.660

In contrast to the dipole transition considered above, these transitions are more significantly affected by atomic potential distortion and channel coupling effects. The PWBOA results differ considerably from the DWA data, indicating a strong influence of the real atomic potential on the scattering processes. For the $3\,^3D$ excitation, the DWA results are very close to those for 5CC, whereas the 19CC values are larger by about 20%. This result can easily be understood because the omission of higher neighboring levels from the close-coupling expansion may have a marked influence. For example, the enhancement of the 19CC cross sections for the quadrupole $(3s^2)^1S$-$(3s3d)^1D$ transition, in comparison to the 5CC data, may result from the two-step virtual process $(3s^2)^1S$-$(3s3p)^1P$-$(3s3d)^1D$, consisting of two strong dipole transitions. This process is taken into account in the present 19CC calculations. As is seen from Table IV, the experimental estimation [11] for the integral cross section agrees closely with present calculated value for an electron energy of 20 eV, but differs considerably from all available calculations at 10 eV.

In the case of monopole transition $(3s^2)^1S$-$(3s4s)^1S$, we see large variations between all of the approximations. This might be expected because as a rule the monopole transitions are the most sensitive to the number of included channels, the accuracy of the target wave functions, and other details of the calculations. Note in this respect that the wave functions for the $3s3d\ ^1D$ and $3s4s\ ^1S$ states are strongly affected by configuration mixing, especially with the $3p^2$ and $3p4p$ configurations.

E. Other transitions from the ground state

Additional comparisons of the calculated results with the experimental data are given in Table V and Figs. 5–7 for excitation to the upper-lying levels. No other theoretical data exist in the literature for comparison in the case of these levels.

First consider the exchange transition $(3s^2)^1S$-$(3s4s)^3S$. Figure 5(a) compares the present results with experiments [2,10], and Fig. 5(b) gives more detailed comparison at low energies with experiment [4]. The relative cross sections from [4] given in this and the next figures are scaled to obtain the best ''visible'' fit to the calculated data. As is seen from Fig. 5(a), the cascade contribution was found to be very important in this case, affecting the emission cross section by up to a factor of 2. This cascade originates mainly from the $3\,^3P$ level. The energy dependence of the emission cross section is in close agreement with both measurements [2] and [10]. The calculated cross section agrees well with the absolute values [10], but differs by a factor of 2 with the absolute values given in [2]. As is seen in Fig. 5(b), there is close agreement at low energies with the high-resolution measurements [4], including the deep hollow at 6 eV. Though the calculated cross sections reveal rich resonance structure, the 6-eV hollow, according to our calculations, is due to the superposition of direct and cascade contributions, and not to a resonance transition, as has been suggested in [4].

We see a similar pattern for the $(3s^2)^1S$-$(3s3d)^3D$ exchange transition in Fig. 6(a) [shown with an enlarged scale in Fig. 6(b)]. The energy dependence of the calculated cross section also agrees qualitatively with all of the experimental data [2,4,10], but the absolute values differ by a factor of 2 for the measurements in [10] and by a factor of 3 for the measurements in [2]. In the case of the $(3s^2)^1S$-$(3s4d)^3D$ transition, Fig. 7(a), the calculated cross section shows an additional broad maximum in the range from 6 to 8 eV in comparison with the measurements [4], and shows no maximum at 10 eV. For the $(3s^2)^1S$-$(3s5s)^3S$ transition, shown in Fig. 7(b), the present calculations reproduce very well the first strong maximum but give overestimated values for the next two maxima. The calculations also show the maximum at 10 eV but shifted to lower energies. The theoretical cross

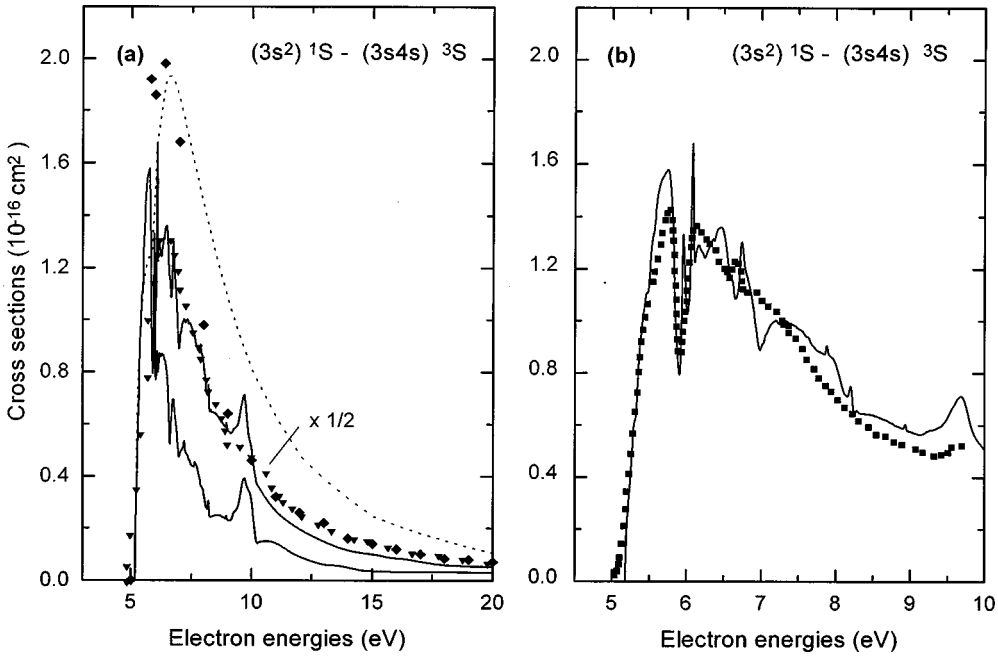

FIG. 5. Comparison of experimental excitation functions with present calculations for the $(3s^2)^1S$-$(3s4s)^3S$ transition in Mg. ——, 19CC results; ------, PWBOA results; ▼, experiment [2]; ■, experiment [4]; ◆, experiment [10].

sections for excitation of the $(3s4d)^3D$ and $(3s5s)^3S$ levels are not likely to be as accurate as those for the other transitions considered before, since these states are on the border of the domain of validity for the close-coupling expansion, and the omission of the higher neighboring levels from the expansion may have a strong influence on these weak exchange transitions.

In contrast to the above-considered exchange transitions, for the spin-allowed transitions $(3s^2)^1S$-$(3s5s)^1S$ [Fig. 7(c)] and $(3s^2)^1S$-$(3s4d)^3D$ [Fig. 7(d)] the calculated energy dependences agree very well with the measurements [2] and [4]. For example, the calculations reproduce the broad and high maximum in the range 6–10 eV for the quadrupole transition $(3s^2)^1S$-$(3s4d)^3D$, which has a sharper appearance in experiment [4], at higher-energy resolution, than in [2]. The absolute values for the $(3s^2)^1S$-$(3s5s)^1S$ transition are in excellent agreement with the measurements [2], whereas for the quadrupole transition $(3s^2)^1S$-$(3s4d)^1D$ the difference for the same measurements is about a factor of 4. This is the largest difference between our theoretical predic-

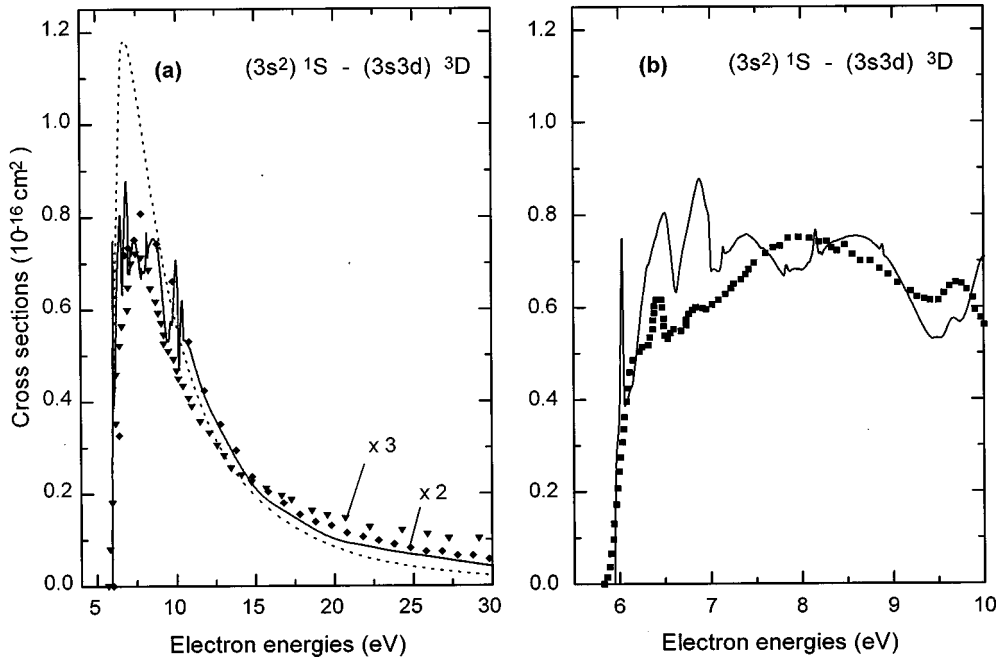

FIG. 6. Comparison of experimental excitation functions with present calculations for the $(3s^2)^1S$-$(3s3d)^3D$ transition in Mg. Notations are the same as in Fig. 5.

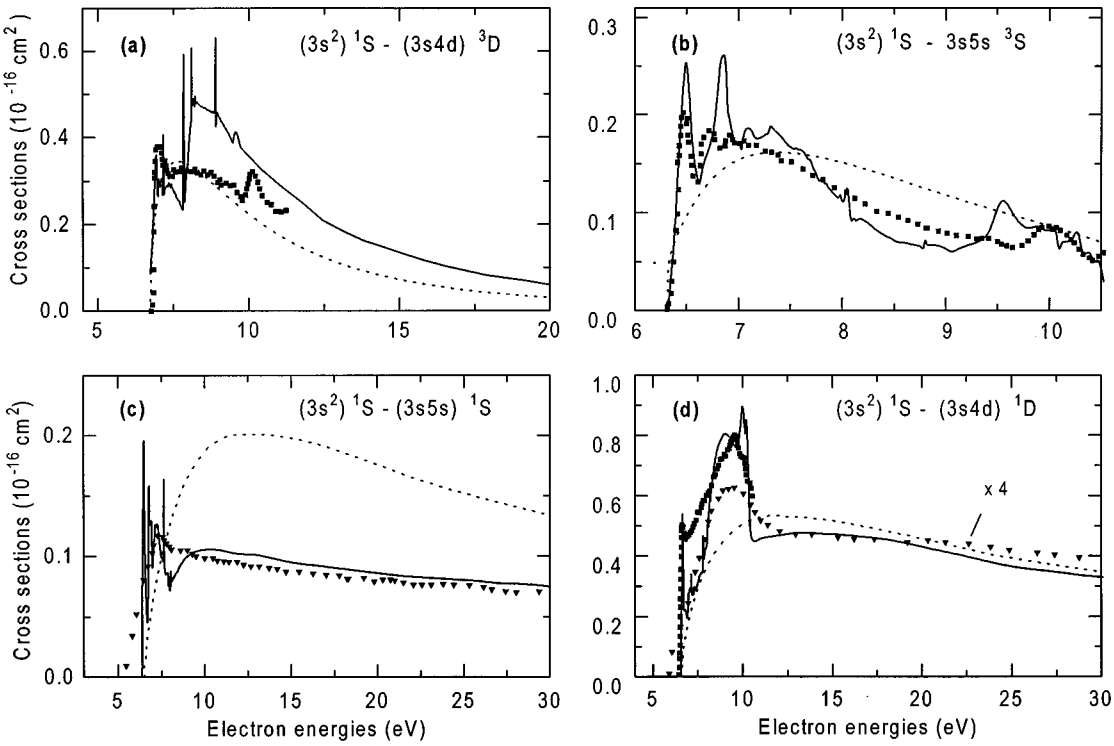

FIG. 7. Comparison of experimental excitation functions with present calculations for some upper-lying levels in Mg. Notations are the same as in Fig. 5.

tions and the experimental data.

F. Transitions from the metastable states

Comparison with the experimental data in the case of excitation from the metastable states $(3s3p)^3P$ can be made from the results shown in Figs. 8(a)–8(d) and Table V. The only experimental group carrying out measurements of excitation from metastable states is that of Shafranyosh [8–10]. The present calculated values of the cross sections are in satisfactory agreement for all transitions except

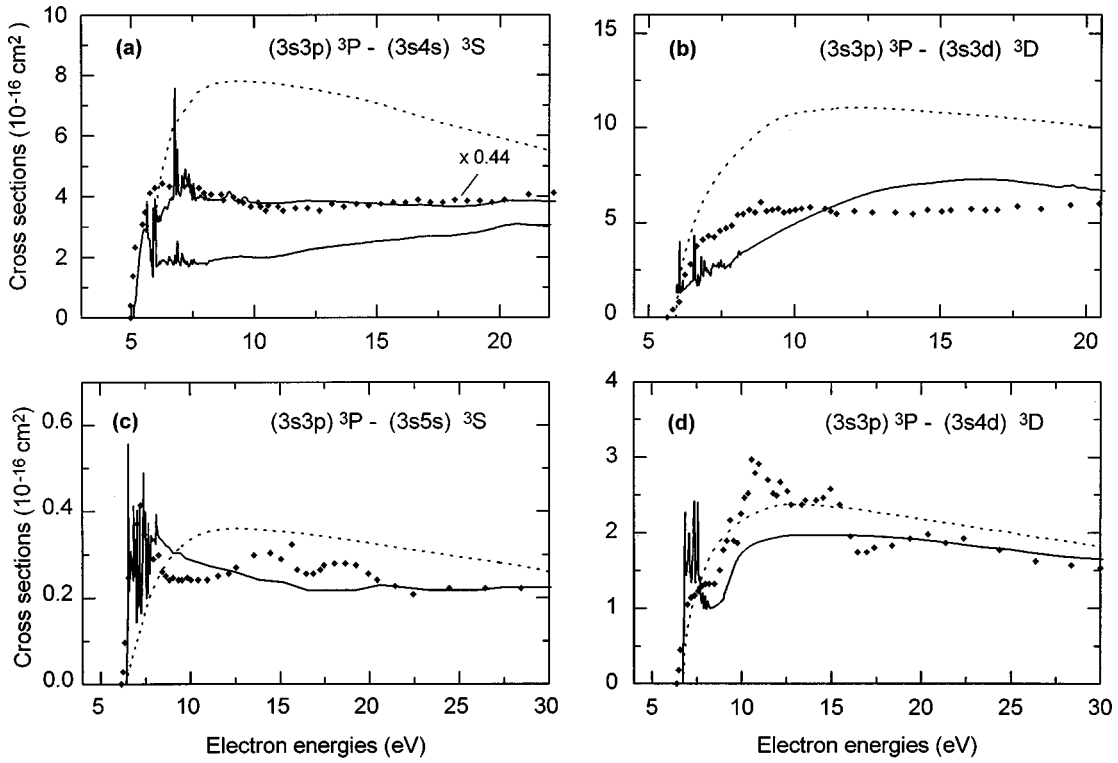

FIG. 8. Excitation cross sections from the 3 ^3P metastable state of Mg as compared with measurements [10]. Notations are the same as in Fig. 5.

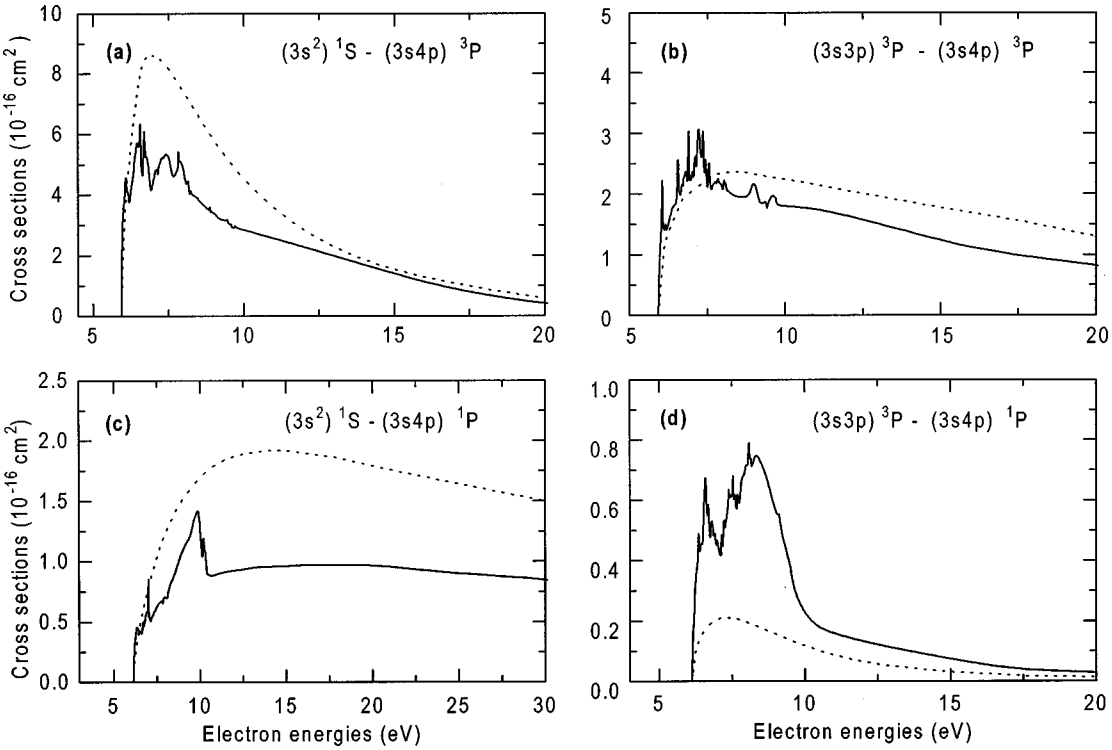

FIG. 9. Comparison of the cross sections for the $(3s4p)^1P$ and $(3s4p)^3P$ levels excited from the ground $(3s^2)$ and metastable $(3s3p)^3P$ states in Mg. Notations are the same as in Fig. 4.

$(3s3p)^3P$-$(3s4s)^3S$, for which the difference is about a factor of 2. On the other hand, the energy dependence for this transition is in close agreement with experiment, whereas other transitions reveal complicated energy dependences which are not reproduced by the calculations. One possible reason can be cascade contributions from the upper levels, not taken into account. An example is given in Fig. 8(a), where the cascade contribution changes considerably the cross section for the $(3s3p)^3P$-$(3s4s)^3S$ transition at low electron energies.

In Figs. 9(a)–9(d) we show how our calculations predict the cross sections for the $(3s4p)^1P$ and ^3P levels for their excitation from both the ground and metastable states. As was mentioned before, these levels play an important role in cascade contributions for S and D levels. The complicated energy dependence of these cross sections at low energies should be noted. As an example, Fig. 9(d) shows the 19CC cross section for the $(3s3p)^3P$-$(3s4p)^1P$ exchange transition, which lies considerably above the PWBOA results, demonstrating the strong influence of close coupling between different states in this case. It is interesting also to note that, as is expected from general considerations, in some cases the cross sections from the metastable state exceed the corresponding cross sections from the ground state and reach magnitudes comparable with those for the resonance transition $(3s^2)^1S$-$(3s3p)^1P$.

IV. SUMMARY AND OUTLOOK

We have presented the results of 19-state close-coupling R-matrix calculations for Mg at low energies. In this first systematic calculation for Mg by the R-matrix method, we have considered excitation from both the ground state and the metastable states. The target states are treated by moderately large configuration-interaction expansions that are fairly successful in describing energies and oscillator strengths. Coupling to the 13 lowest-energy states is treated exactly; coupling to the other bound states and to the continuum is treated by the inclusion of six pseudostates, one for each angular symmetry of the target. The continuum is found to have a large influence, and the inclusion of pseudostates substantially affects the shape and magnitude of the excitation cross sections at low and intermediate energies. We also find that the inclusion of pseudostates considerably reduces the pseudoresonance structure which is an inherent feature of R-matrix calculations for two-electron atoms.

The calculated cross sections have been used in the interpretation of all available experimental data, with most attention being devoted to the absolute values of the integral cross sections. For most of the experimental data [2,7,10] this was the first comparison with theoretical calculations. Close agreement with experiments was obtained for the resonant $(3s^2)^1S-3s3p\ ^1P$ and elastic cross sections, including the near-threshold resonance structure. There is also good agreement for the most transitions to the upper states, but for some exchange and monopole transitions the difference can be as large as a factor of 2 to 4. We note here that to obtain accurate experimental cross sections is quite difficult, as Mg requires high temperatures for vaporization. As a result, the estimation of the number of Mg atoms in the scattering chamber is a difficult task. In the comparison of the theoretical and experimental emission cross sections, the cascade contribution was also found to be very important. On the other hand, the energy dependence of all of the calculated cross sections is in very good agreement with the measure-

ments, providing additional evidence in support of the accuracy of these calculations. Therefore our theoretical results for a variety of transitions might be used for normalizing experimental data. Further experimental and theoretical efforts seem worthwhile and are required before this collision system will be fully understood.

Satisfactory agreement was obtained with the coupled-channel optical calculations (6CCO, [15]), whereas as expected the first-order approximations DWA and PWBOA show large discrepancies at low energies. These results demonstrate the significant close-coupling effects in electron scattering by Mg. Nevertheless, the simple PWBOA, in conjunction with accurate target wave functions, gives rather accurate cross sections at intermediate energies for both spin-allowed and spin-forbidden transitions.

For electron-impact excitation of Mg, most of the calculated cross sections display complicated near-threshold behavior that reveals a rich resonance structure. What we have in mind are resonances due to the formation of autodetached states of the negative Mg^- ion, in states such as $3s3p^2$, $3s3p4s$, or $3s4s^2$, which are formed via temporary capture of the incident electron by the excited Mg target. Detailed examination of this resonance structure will be described in further publications. The differential cross sections are another very interesting topic beyond the scope of the present calculations. The comparison of the theoretical and experimental differential cross sections can reveal much more about the accuracy of the approximations used in these scattering calculations. In the near future we expect to perform calculations for the examination of the available experimental differential cross sections.

ACKNOWLEDGMENTS

The present study was supported in part by the International Science Education Program of the International Renaissance Foundation under Grant Nos. SPU042037 and QSU082069, and by the Ministry of Education of Ukraine under Grant No. UDB-264. We appreciate the help of T. A. Zatsarinny and Dr. S. P. Bogacheva in carrying out numerical calculations.

[1] H. P. Summers *et al.*, Plasma Phys. Controlled Fusion **34**, 325 (1991).
[2] I. S. Aleksahin, I. P. Zapesochnyi, I. I. Garga, and V. P. Starodub, Opt. Spektrosk. **34**, 1053 (1973) [Opt. Spectrosc. **34**, 611 (1973)].
[3] D. Leep and A. Gallagher, Phys. Rev. A **13**, 148 (1976).
[4] O. B. Shpenik, I. P. Zapesochnyi, E. E. Kontrosh, E. I. Nepijpov, N. I. Romanyuk, and V. V. Sovter, Zh. Eksp. Teor. Fiz. **76**, 846 (1979) [Sov. Phys. JETP **49**, 426 (1979)].
[5] W. D. Robb, J. Phys. B **7**, 1006 (1974).
[6] P. D. Burrow and J. Comer, J. Phys. B **8**, L92 (1975); see also P. D. Burrow, J. A. Michejda, and J. Comer, *ibid.* **9**, 3225 (1976).
[7] N. I. Romanyuk, O. B. Shpenik, A. I. Zhukov, and I. P. Zapesochnyi, Pis'ma Zh. Tekh. Fiz. **6**, 877 (1980).
[8] I. I. Shafranyosh, T. A. Snegurskaya, and I. S. Aleksakhin, Opt. Spektrosk. **68**, 262 (1990) [Opt. Spectrosc. **68**, 152 (1990)]; **76**, 20 (1994) [**76**, 23 (1994)]; I. I. Shafranyosh, T. A. Snegurskaya, and M. O. Margitich, *ibid.* **77**, 725 (1994) [**77**, 646 (1994)].
[9] I. I. Shafranyosh, T. A. Snegurskaya, M. O. Margitich, S. P. Bogacheva, V. I. Lengyel, and O. I. Zatsarinny, J. Phys. B **30**, 2261 (1997).
[10] T. A. Snegurskaya, Ph.D. thesis, Uzhgorod State University, 1993; I. I. Shafranyosh (private communication).
[11] W. Williams and S. Trajmar, J. Phys. B **11**, 2021 (1977); M. J. Brunger, J. L. Riley, R. E. Scholten, and P. J. O. Teubner, *ibid.* **21**, 1639 (1988); **22**, 1431 (1989).
[12] R. K. Houghton, M. J. Brunger, G. Shen, and P. J. O. Teubner, J. Phys. B **27**, 3573 (1994).
[13] S. Kaur, R. Srivastava, R. P. McEachran, and A. D. Stauffer, J. Phys. B **30**, 1027 (1997).
[14] I. I. Fabrikant, J. Phys. B **13**, 603 (1980).
[15] J. Mitroy and I. E. McCarthy, J. Phys. B **22**, 641 (1989).
[16] I. E. McCarthy, K. Ratnavelu, and Y. Zhou, J. Phys. B **22**, 2597 (1989).
[17] R. E. H. Clark, G. Csanak, and J. Abdallah, Phys. Rev. A **44**, 2874 (1991).
[18] *Atoms in Astrophysics*, edited by P. G. Burke, W. Eissner, D. Hummer, and L. Percival (Plenum, New York, 1983).
[19] K. Bartschat, E. T. Hudson, P. G. Burke, M. P. Scott, and V. M. Burke, J. Phys. B **29**, 115 (1996).
[20] K. Bartschat, P. G. Burke, and M. P. Scott, J. Phys. B **30**, 5915 (1997).
[21] P. G. Burke and W. D. Robb, Adv. At. Mol. Phys. **11**, 143 (1975).
[22] I. Bray and A. T. Stelbovics, Phys. Rev. A **46**, 6995 (1992).
[23] I. Bray and A. T. Stelbovics, Adv. At., Mol., Opt. Phys. **35**, 209 (1995).
[24] D. V. Fursa and I. Bray, J. Phys. B **30**, 757 (1997).
[25] D. V. Fursa and I. Bray, J. Phys. B **30**, 5895 (1997).
[26] D. V. Fursa and I. Bray (unpublished).
[27] V. Gedeon, V. Lengyel, O. Zatsarinny, and C. A. Kocher, Phys. Rev. A **56**, 3753 (1997).
[28] O. I. Zatsarinny, V. I. Lengyel, and E. A. Masalovich, Phys. Rev. A **44**, 7343 (1991).
[29] V. I. Lengyel, V. T. Navrotsky, and E. P. Sabad, *Resonance Phenomena in Electron-Atom Collisions* (Springer, Heidelberg, 1992).
[30] K. A. Berrington, W. B. Eissner, and P. Norrington, Comput. Phys. Commun. **92**, 290 (1995).
[31] P. J. Marchalant and K. Bartschat, J. Phys. B **30**, 4373 (1997).
[32] M. I. Haysak, L. A. Bandurina, M. M. Dovganich, and O. I. Zatsarinny, Laser Phys. **7**, 766 (1997).
[33] W. C. Martin and R. Zalibas, J. Phys. Chem. Ref. Data **9**, 1 (1980).
[34] C. Froese Fischer, Can. J. Phys. **53**, 184, 338 (1975).
[35] (a) L. Liljeby, A. Lindgard, S. Manervik, E. Veje, and B. Jelemkovic, Phys. Scr. **21**, 805 (1980); (b) F. M. Kelly and M. S. Mathur, Can. J. Phys. **58**, 1980 (1980); (c) L. Lundin, B. Engman, J. Hilke, and I. Martinson, Phys. Scr. **8**, 274 (1973);

(d) W. W. Smith and A. Gallagher, Phys. Rev. **145**, 26 (1966); (e) W. W. Smith and H. S. Liszt, J. Opt. Soc. Am. **61**, 938 (1971); (f) T. Andersen, J. Sesesquelles, K. A. Jessen, and G. Sorenson, J. Quant. Spectrosc. Radiat. Transf. **10**, 1143 (1970); (g) C. J. Mitchell, J. Phys. B **8**, 25 (1975); (h) A. Schaefer, Astrophys. J. **163**, 411 (1971).

[36] K. Meyer, C. H. Greene and I. Bray, Phys. Rev. A **52**, 1334 (1995).